The Effect of Processing Conditions on Structure Evolution in Melt Spun Poly(Ethylene Terephthalate) Fibers

M. J. NAPOLITANO and A. MOET, *Department of Macromolecular Science, Case Western Reserve University, Cleveland, Ohio 44106*

Synopsis

An investigation has been made into the structural evolution in poly(ethylene terephthalate) fibers as a function of wind-up speed (WUS) and quench air temperature (QAT). Analysis of the mechanics and mechanisms of cold drawing reveals that the fiber structure is heterogeneous. Evidence from differential scanning calorimetry (DSC) and density measurements indicates the presence of crystallites which are imperfect according to wide-angle diffraction (WAXD). Increased thread-line stress (higher WUS and higher QAT) appears to induce larger and more oriented crystallites in a progressively oriented matrix. A radially layered structure is disclosed from high resolution scanning electron microscopy (SEM) micrographs.

INTRODUCTION

Several process variables influence the ultimate properties of melt spun poly(ethylene terephthalate) (PET) fibers. These include molecular weight of the polymer, spinning temperature, cooling rate, volume throughput, wind-up speed (WUS), and tooling configuration.[1] A competition between molecular relaxation and stress-induced ordering underlies structural evolution in the spun fiber. The quest to achieve highly ordered structures at increased production rates led to the development of spinning lines with wind-up speeds up to 10,000 m/min.[2] Elevated wind-up speeds result in higher fiber stress.[3] This, in turn, enables ordering processes to overcome molecular relaxation in the vicinity of the freezing point and produces threadline crystallization.[3] A transition in the fiber structure is reported to occur in a WUS range of 3500–4500 m/min.[4,5] Below this speed, the fiber structure is believed to be essentially amorphous whose orientation increases with WUS.

Annealing studies, however, suggest that nucleation of crystallites is probable at WUS as low 1600 m/min and that this probability increases with WUS.[6] Subsequent investigations imply the formation of a "mesophase" in fibers spun at speeds of 1000 to 2400 m/min.[7] Clearly, the structure of PET fibers spun at low speeds remains controversial. Although high degrees of crystallinity have been measured for fibers spun at higher speeds,[8] the nature of the crystalline structures themselves is still controversial.

This paper reports on the results of a concerted characterization effort to identify evolving structures in PET fibers spun in the range of 500–2500

Journal of Applied Polymer Science, Vol. 32, 4989–5006 (1986)
 CCC 0021-8995/86/054989-18$04.00

m/min. In addition to conventional characterization techniques, analysis of the mechanical behavior and deformation mechanisms is employed to unveil the structures present.

EXPERIMENTAL

Materials

PET fibers were produced by melt spinning at wind-up speeds ranging from 500 to 2500 m/min at quench-air temperatures of 23°C and 40°C. The number average molecular weight was 32,000 with a molecular weight distribution of approximately 2. The die temperature, volumetric throughput, and the die geometry were held constant. Each of the fibers produced was of variable denier (Fig. 1).[9] The fibers examined are identified by their wind-up speed (WUS)/quench-air temperature (QAT).

MECHANICAL TESTING

Stress–strain experiments were performed on an Instron testing machine at room temperature in air. Ten specimens were tested in each experiment and the data reported are statistical averages of the 10 specimens. The

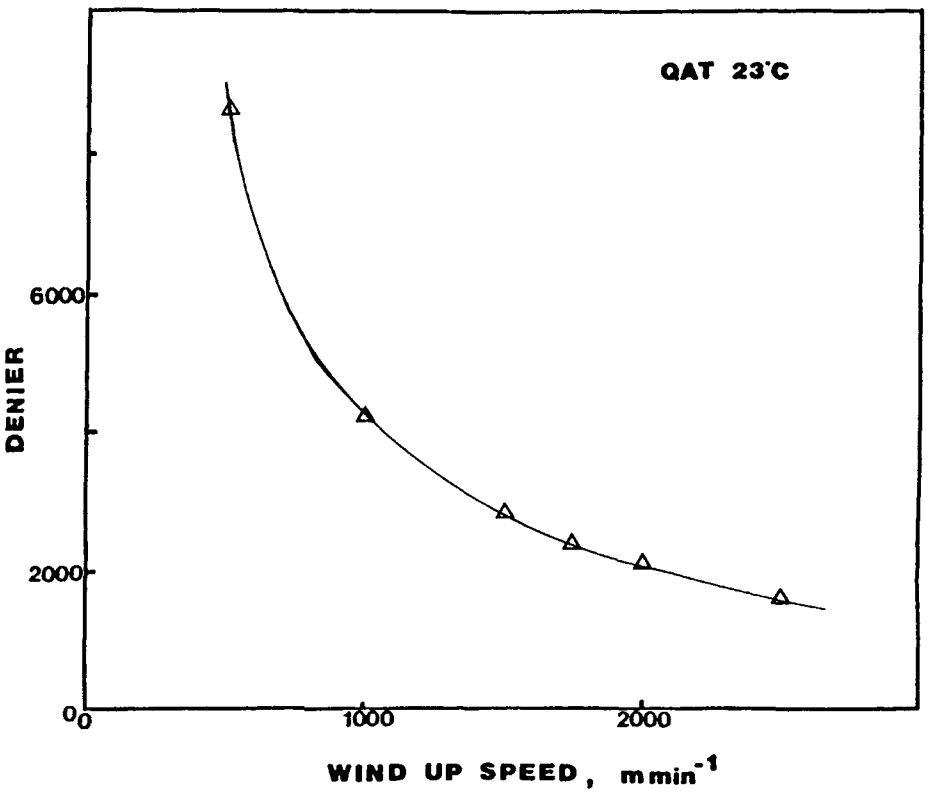

Fig. 1. The effect of wind-up speed on the as-spun fiber denier at a quench-air temperature of 23°C.

materials were tested at a strain rate of 20%/min using adhesive tape with pneumatic clamps as grips. A gauge length of 170 mm was selected to minimize grip effects. The variation of the modulus of the fibers with gauge length was studied and the modulus achieved a stable, reproducible value for gauge lengths above 150 mm (Fig. 2). The force applied to the fiber is normalized by dividing by the fiber denier. In Figure 1, it is observed that the denier of the fibers increased as the spinning speed decreased.[9]

OPTICAL MICROSCOPY

Birefringence measurements were made on an Aus Jena Interphako interference microscope using an Ehringhuas compensator calibrated to green light (λ = 551 nm). Twenty single filaments were randomly taken from the fiber bundle for birefringence and radius measurements. The reported birefringence and radius values are averaged over the number of samples tested. To improve the visual observation of the extinction band and to get an accurate measure of the thickness, the fibers were immersed in mineral oil which has a similar refractive index. Fibers were also examined in transmitted and crossed polarized light for deformation mechanisms.

X-RAY DIFFRACTION

A Statton camera attached to a Phillips X-ray source of 40 kV was used to record the wide-angle diffraction (WAXD) patterns from the as-spun fibers. The fibers were mounted on a rack under slight tension to improve

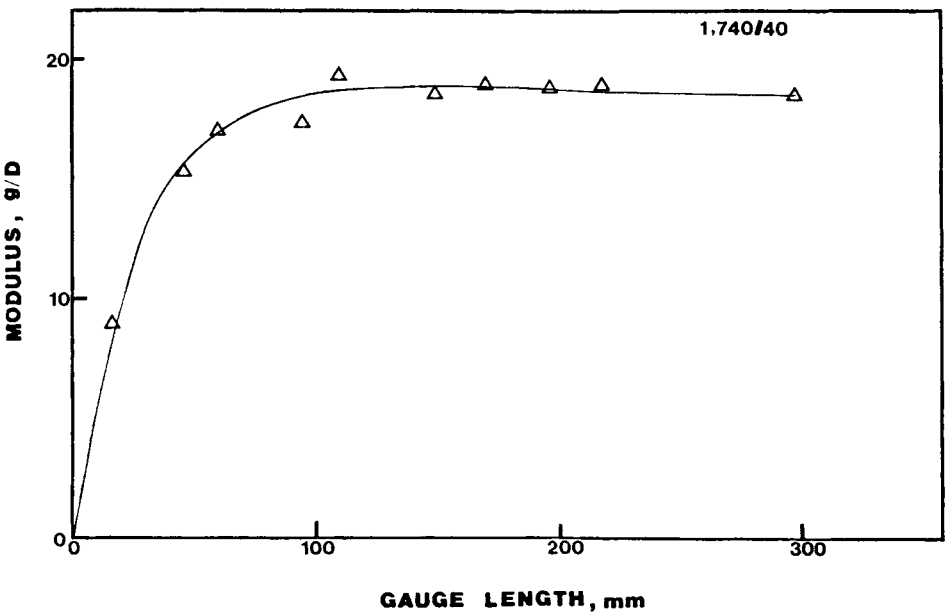

Fig. 2. The dependence of the elastic modulus on the gauge length of PET fiber sample spun at 1750 m/min and a quench-air temperature of 40°C cold drawn at 20%/min at room temperature.

the alignment of the filaments in the beam path. All patterns were taken with the fiber axis normal to the X-ray beam.

CALORIMETRIC ANALYSIS

A Perkin Elmer DSC-II was used for the calorimetric analysis of the spun fibers. The fibers were cut into pieces of about 1–3 mm in length to minimize the effect of fiber shrinkage upon heating.[10] The specimens were heated at a rate of 20°C/min between 300°K and 550°K. The average sample weight was about 3.5 mg. All results reported are an average from five runs. The glass transition temperature was taken as the midpoint of the slope of the transition in heat capacity.

DENSITY

The density of the as-spun fibers was measured using a density gradient column constructed according to ASTM D1505. The temperature of the column was held at a constant 23°C. Carbon tetrachloride (ρ = 1.5487 g/cc) and *n*-heptane (ρ = .6837 g/cc) were used to construct a gradient column of the appropriate density range (1.30–1.40 g/cc). The as-spun fibers were washed in carbon tetrachloride then vacuum dried for 24 h at room temperature. The density reported is an average of five density measurements.

RESULTS

The wind-up speed is a machine variable which effects the level of tension on the threadline during the spinning. Since the volumetric throughput is constant, the spinning speed will influence the radius of the as-spun fiber. The average filament radius is plotted as a function of the wind-up speed in Figure 3. The average radius is reduced from 25 μm to about 10 μm in the range of wind-up speeds examined. The relationship between the radius of the fibers and the wind-up speed does not appear to deviate from monotonic behavior. There is a slight tendency to obtain thinner filaments at 40°C quench-air temperature. However, the effect of this temperature range is negligible compared to that of the spinning speed.

The level of stress produced in the threadline during melt spinning is one of the major driving forces for structural evolution. This is a direct manifestation of the wind-up speed and the fiber temperature. These, however, depend on the configuration of the particular spinning unit and operational conditions such as melt temperature, spinnerette design, and molecular weight of the polymer. Thus, it is instructive to relate process variables to the birefringence of the fiber as an acceptable structural parameter. Although the birefringence is a crude measure of the complex structure evolving in melt spun fibers, it serves to classify fibers spun under variable QAT and WUS. In Figure 4, the average birefringence is plotted versus the wind-up speed for the two quench-air temperatures. Limited orientation is achieved below spinning speeds of 1000 m/min, irrespective of the quench-air temperature. Above 1000 m/min, the rate of increased orientation is highly enhanced particularly at the higher quench air temperature. Similar re-

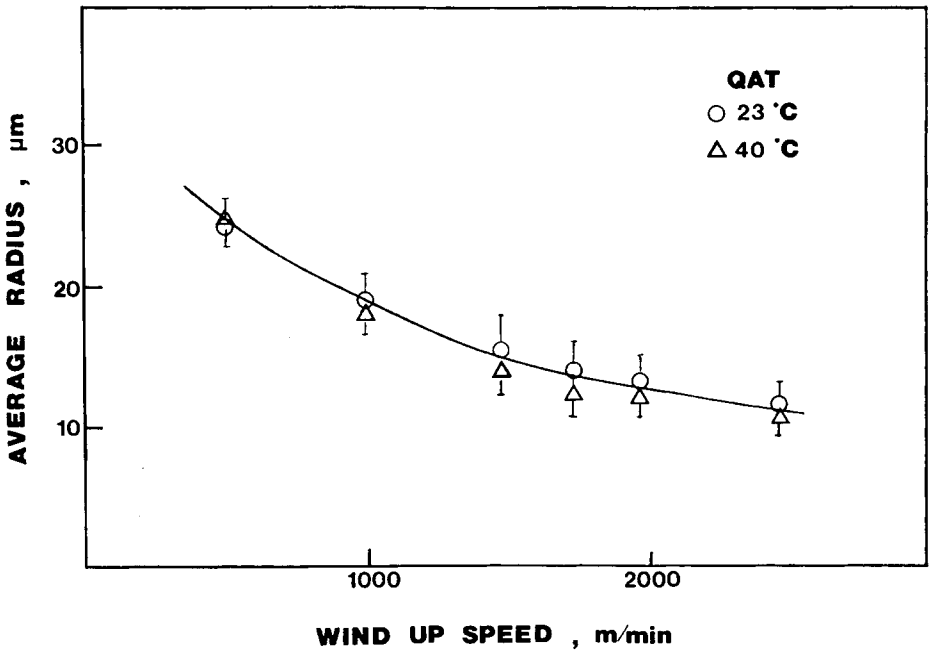

Fig. 3. Average radius versus wind-up speed and the quench-air temperature.

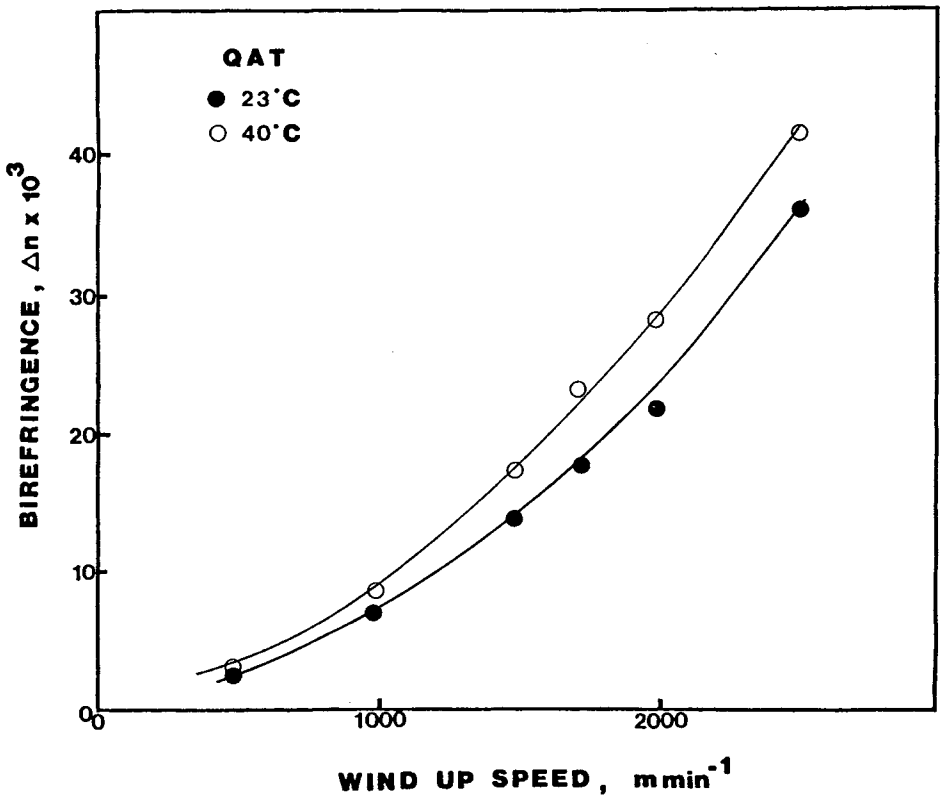

Fig. 4. Birefringence versus wind-up speed and the quench-air temperature.

lationships have been observed between birefringence and wind-up speed,[4,11-13] but due to the fact that the birefringence is dependent not only on the wind-up speed, but on other operational variables, direct comparison with other researchers is not possible, although a qualitative agreement is observed.

The wide-angle X-ray patterns from the as-spun fibers produced at different processing conditions are presented in Figure 5. All patterns show no clear indication of well developed crystalline regions. This is evident from the large amorphous halo and the lack of any distinct diffraction bands. WAXD patterns for fibers spun above 1000 m/min, however, shows intensification of the amorphous halo along the equatorial line (see pattern 2500/40 of Fig. 5) with the intensification increasing as the wind-up speed increases. This intensification may be caused by a preferred orientation of the amorphous material with respect to the fiber axis or the presence of small crystallites in the fiber. Similar WAXD patterns for melt spun fibers has been observed for PET fibers spun under similar conditions.[4,7,14,15]

In order to obtain more specific information on the structural state of the as-spun fibers, calorimetric analysis was done. Figure 6 presents typical thermograms obtained from the as-spun fibers. The glass transition tem-

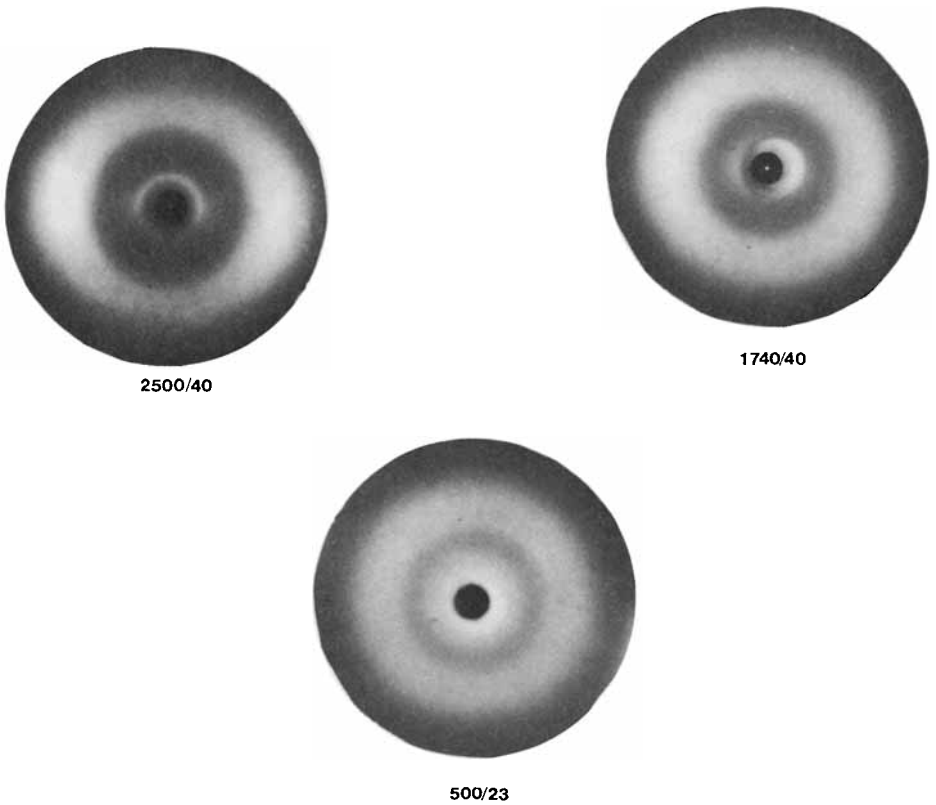

Fig. 5. WAXD of the as-spun fibers processed at various conditions. Fibers are identified by their wind-up speed/quench-air temperature with an intensification noted along the equator at higher wind-up speed.

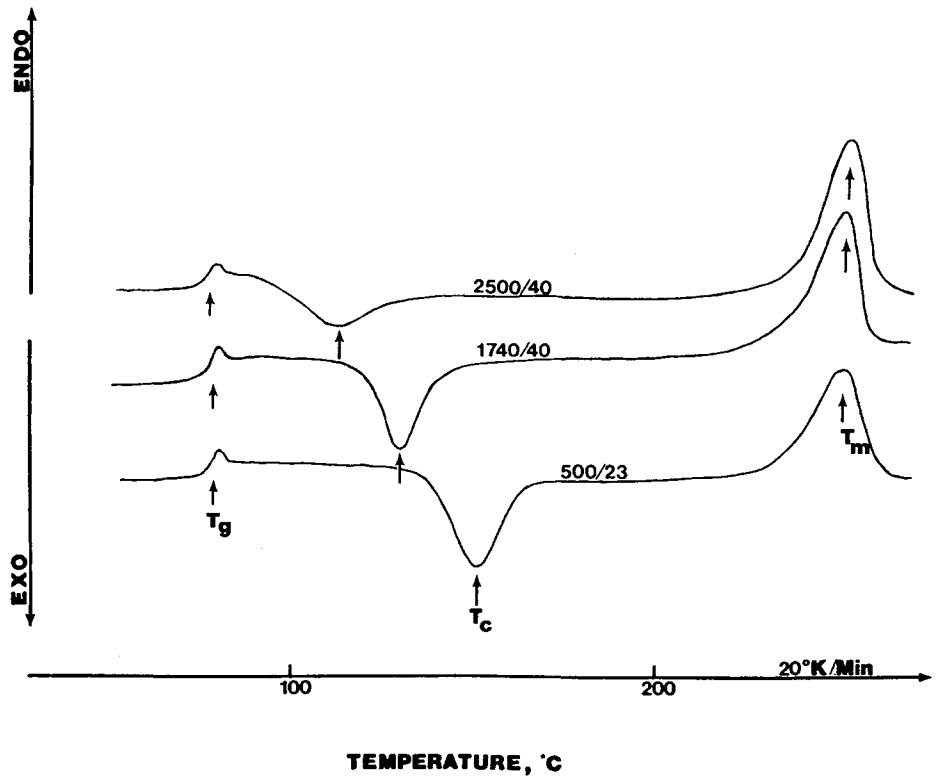

Fig. 6. DSC thermograms of as-spun fibers. Fibers are identified by their wind-up speed/quench-air temperature. A decrease in the cold crystallization temperature (T_c) is seen as the wind-up speed increases.

perature (T_g) for the three fiber samples was observed at 73.5°C and appears independent of the processing conditions. The differential scanning calorimetry (DSC) traces indicate that the processing conditions influence the cold crystallization behavior considerably. At high levels of orientation, the cold crystallization is shifted to lower temperatures. In Figure 7, the cold crystallization temperature is plotted versus the wind-up speed and birefringence. Fibers spun at lower speeds display higher cold crystallization temperature. Again, the QAT range used does not greatly affect the cold crystallization behavior. This tendency is in agreement with the observation of Heuvel and Huisman.[4] A change is also observed in the shape of the cold crystallization exotherm. At higher orientations the cold crystallization process takes place over a wider temperature range than those observed for fibers of lower orientation. The melting behavior, on the other hand, appears to be independent of the processing conditions. A melting endothermic peak was observed at 249 ± 1.2°C for all three samples. A quantitative analysis of the area under the melting endotherms and cold crystallization exotherms shows that more energy is associated with the melting transition. This energy difference is observed to increase with increased fiber preorientation. The area under the endotherm represents the energy associated with melting of the crystallites formed during the scan and the melting of any crys-

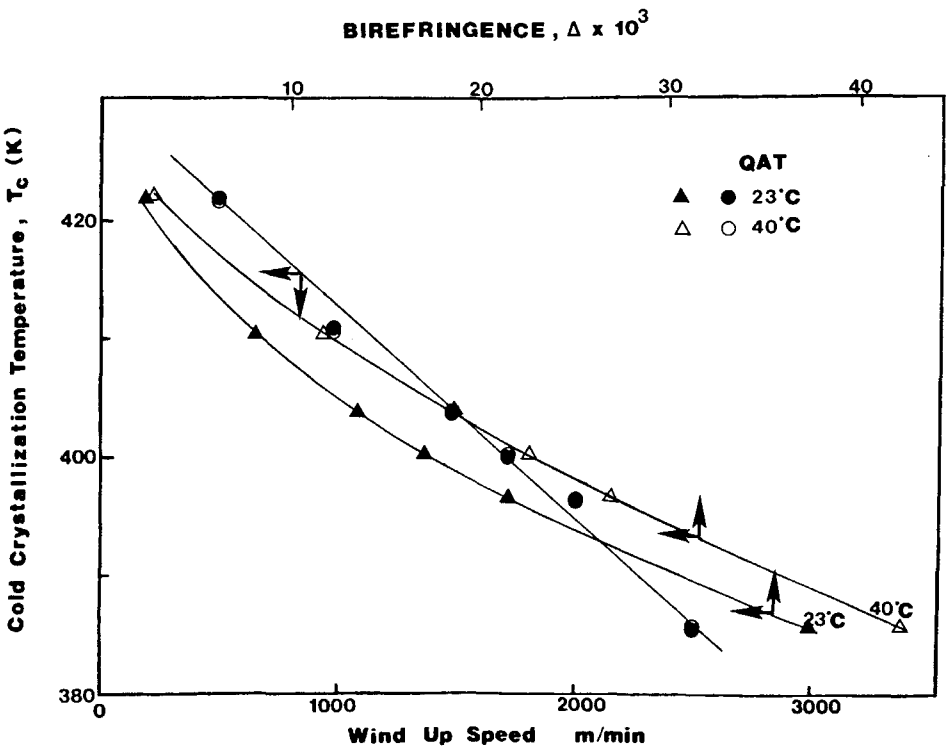

Fig. 7. The effect of wind-up speed and quench-air temperature on the cold crystallization temperature. The cold crystallization temperature is also plotted versus the initial birefringence of the as-spun fiber.

talline material already present in the fiber. In addition, the melting and recrystallization of crystallites formed at lower temperatures and any internal reorganization which may take place during the scan will effect the area under the endotherm.[16] Noticeable recrystallization of PET is reported to occur at scanning rates below 16°/min.[17] At our scanning rate (20°/min) this effect should be negligible.

The density of the as-spun fibers is presented in Figure 8. The density increases as the wind-up speed is increased. A noticeable increase in the density is observed to occur at spinning speeds of 2500 m/min. Similar increases are reported to occur around 3500 m/min.[3,4,6,13,18-20] This transitional speed is known to depend on molecular weight[15] and processing variables.[3] When all processing variables are held constant, the transitional speed is known to decrease with increasing molecular weight.[3] In view of the fact that our material is of higher molecular weight than those used in previous studies,[3,4,6,13,18-20] it is therefore plausible that our transitional speed should be lower. It is also observed (Fig. 8), that for any given wind-up speed the fiber processed at the higher quench-air temperature has a higher density. The QAT-induced density change becomes larger at higher wind-up speed.

The mechanical properties and the drawing mechanism are strongly influenced by the anisotropy induced during the spinning process. Three rep-

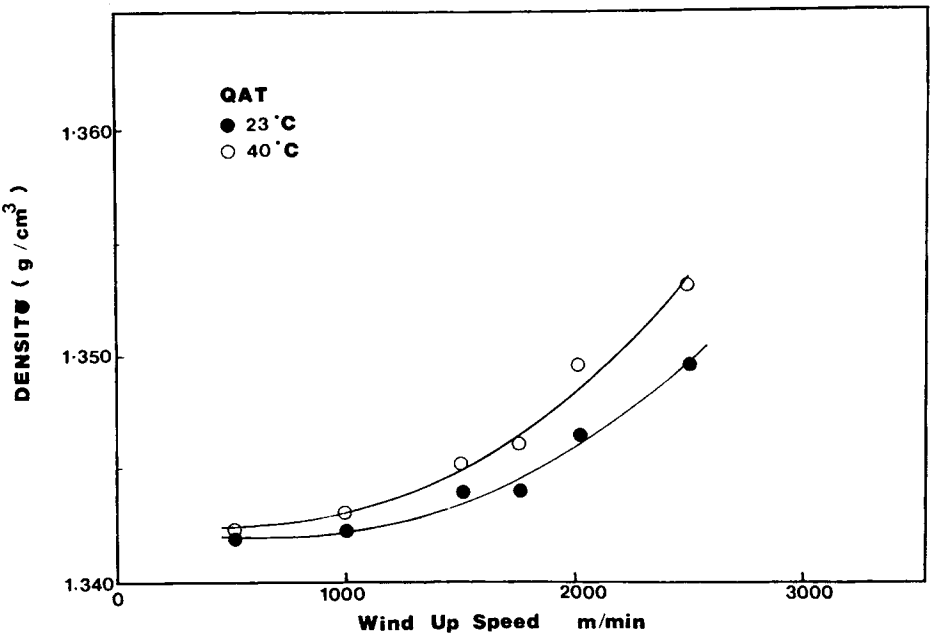

Fig. 8. The density of the as-spun fiber as measured in a density gradient column as a function of wind-up speed at two different quench-air temperatures.

resentative stress-strain curves, recorded at a strain rate of 20%/min, are shown in Figure 9. There is an observed increase in the modulus, yield stress, and draw stress with increasing wind-up speed. Discontinuous neck propagation is observed in fiber sample 500/23 during the cold-drawing process which results in an oscillating stress-strain relationship at this strain rate and gauge length. Similar oscillatory behavior has been observed in the cold drawing of PET.[21,22] The neck oscillates between regions of neck instability and resistance to neck propagation. Concurrently with this instability, intense whitening was observed in the unnecked portion of the sample. The whitening in the unnecked material appears to be related to the formation of localized deformation zones normal to the applied stress (Fig. 10). The formation of these deformation zones is dominant in fibers spun below 1000 m/min. Fiber spun above 1000 m/min experiences only a shear yield phenomena with no formation of local deformation zones observed (Fig. 11).

In general, all fibers yield at about 2.5% elongation, then exhibit a region of constant-load plastic deformation during which neck propagation occurs. When the neck has propagated over the entire gauge of the sample, the drawn fiber experiences a redrawing process marked by a sharp increase in the stress-strain coefficient. The elastic modulus, yield stress, the magnitude of constant-stress drawing (i.e., the natural draw ratio), clearly reflect the initial state of the as-spun fiber. In Figure 12, the initial modulus is plotted versus the average initial orientation as depicted by birefringence. For fibers of high orientation the modulus is 25.2 ± 0.4 g/D, and the modulus of low orientation is 14.7 ± 0.44 g/D. These results follow the trend reported earlier for fibers of similar orientation[23] and over a wider range of orientation.[18]

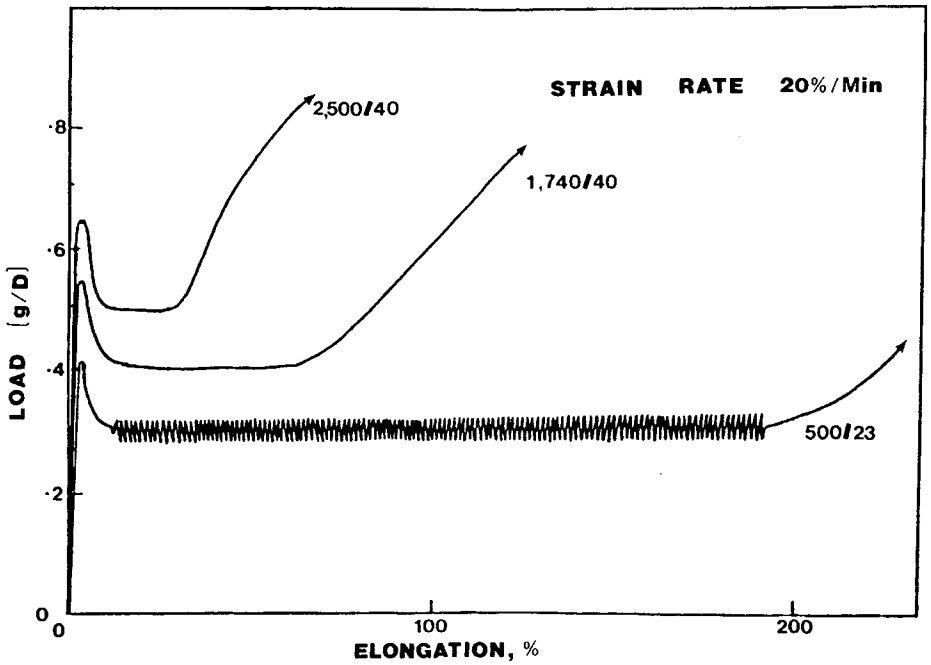

Fig. 9. Typical stress-strain curves of three representative as-spun fibers drawn at room temperature at 20%/min. The fibers are identified by their wind-up speed/quench-air temperature.

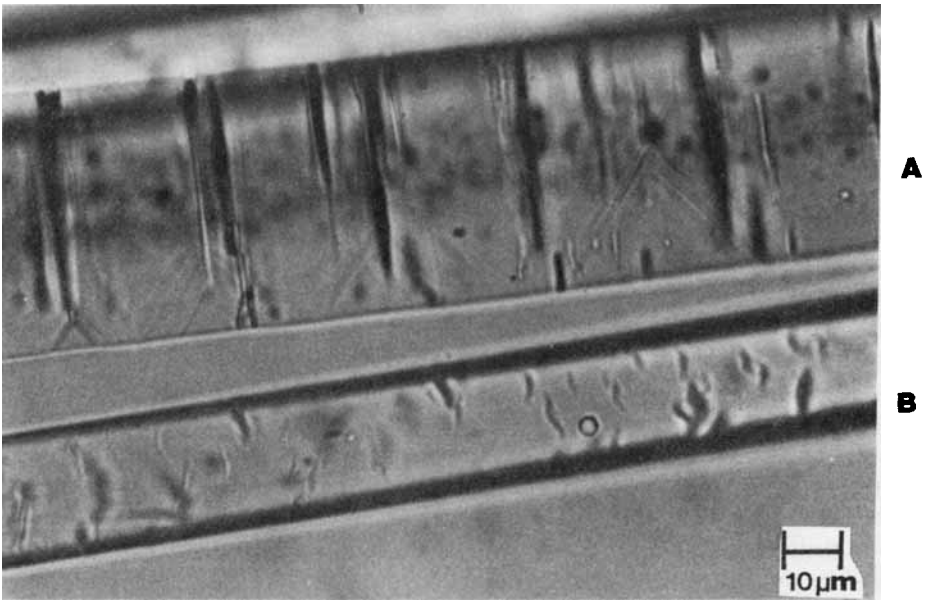

Fig. 10. Transmission optical micrograph of fibers spun at 500 m/min and at a quench-air temperature of 23°C. Normal deformation bands (a), prior to neck formation (b).

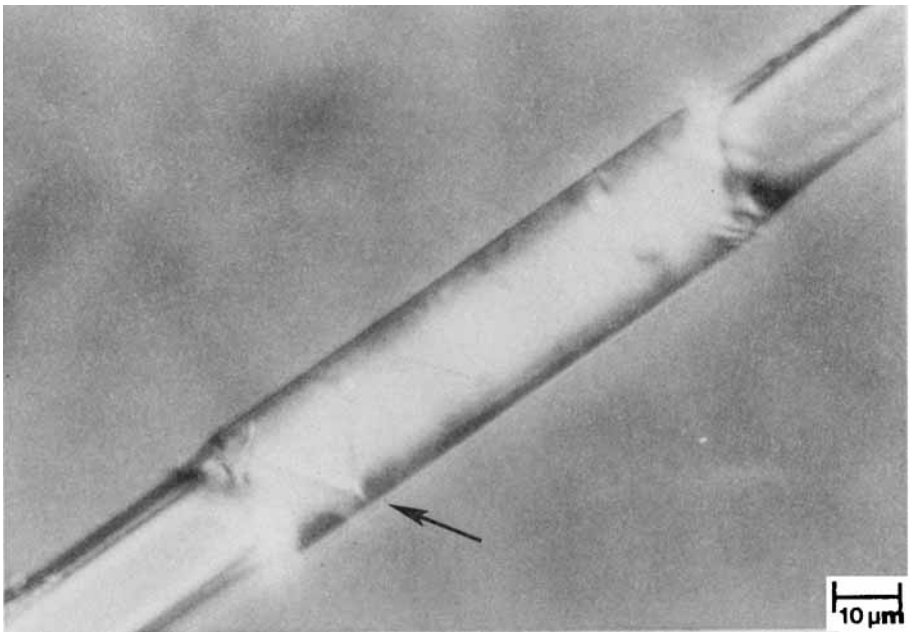

Fig. 11. Transmission optical micrograph of fibers spun at 2500 m/min and at a quench-air temperature of 40°C elongated 3% at 20%/min strain rate showing shear bands (arrow) prior to neck formation.

The increase in the modulus is proportional to the increase in level of total orientation present in the fiber as measured by the birefringence. A similar linear relationship between birefringence and the draw and yield stresses is observed in Figure 13. The natural draw ratio, however, decreases exponentially with the birefringence (see Fig. 14). Fibers of low orientation exhibit a natural draw ratio of 3.0, compared to a value of 1.28 for fibers of higher initial orientation. Notably, the magnitude of the observed modulus increase is nearly equal to the decrease in the natural draw ratio.

The suprastructure of the as-spun filaments was investigated by analysis of the fracture surface of a single filament fractured in liquid nitrogen (Fig. 15). The development of a distinct radial structure is evident by the steps present on the fracture surface.

DISCUSSION

The aim of this study is to identify the structural entities developed in PET fibers spun in the range of 500–2500 m/min and how do such entities evolve as a function of spinning speed (WUS) and quench-air temperature (QAT). In this respect, it is useful to recall that PET can be ultraquenched into its amorphous state[24] or can be caused to form a single crystal.[25] Rapidly quenched PET has been shown to develop nodular domains in the order of ca. 100 Å.[19,25] The specific structure of the domain morphology is not yet resolved. Due to the strong tendency of the polymer to crystallize, these

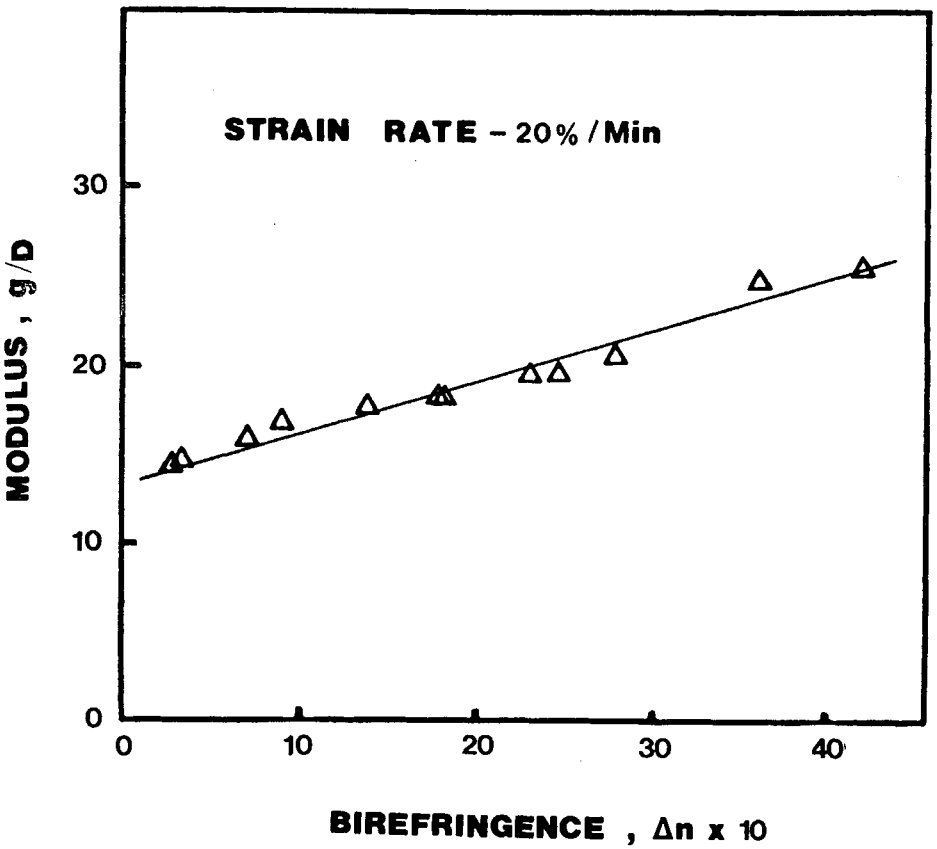

Fig. 12. Initial modulus-birefringence interrelationship for fibers drawn at room temperature at 20%/min.

domains may be considered ordered material of less developed crystalline nature.

In a recent publication, Lindenmeyer analyzed the melt spinning of fiber within a framework of Onsager thermodynamics of irreversible processes.[26] The author draws a conclusion that fiber formation is an unstable dissipative process which should yield a heterogeneous structure. Thus, the idea of heterogeneous structure may not be ruled out.

Collectively, results of the eight different approaches presented in the previous section indicate that the structure of the fibers spun at all speeds examined, involves at least two domains. The evidence obtained from each experiment is discussed below.

The overall orientation reflected in the birefringence rise (Fig. 4) and the modulus increase (Fig. 12) as a function of increased spinning speed can be interpreted in terms of two different hypotheses. The first model is a purely amorphous structure whose orientation increases with wind-up speed and at a critical wind-up speed threadline crystallization takes place in the oriented amorphous material. A second possible hypothesis is that there is a continuous evolution of oriented crystallites in a progressively oriented matrix over the entire range of spinning speeds. It is not possible to dis-

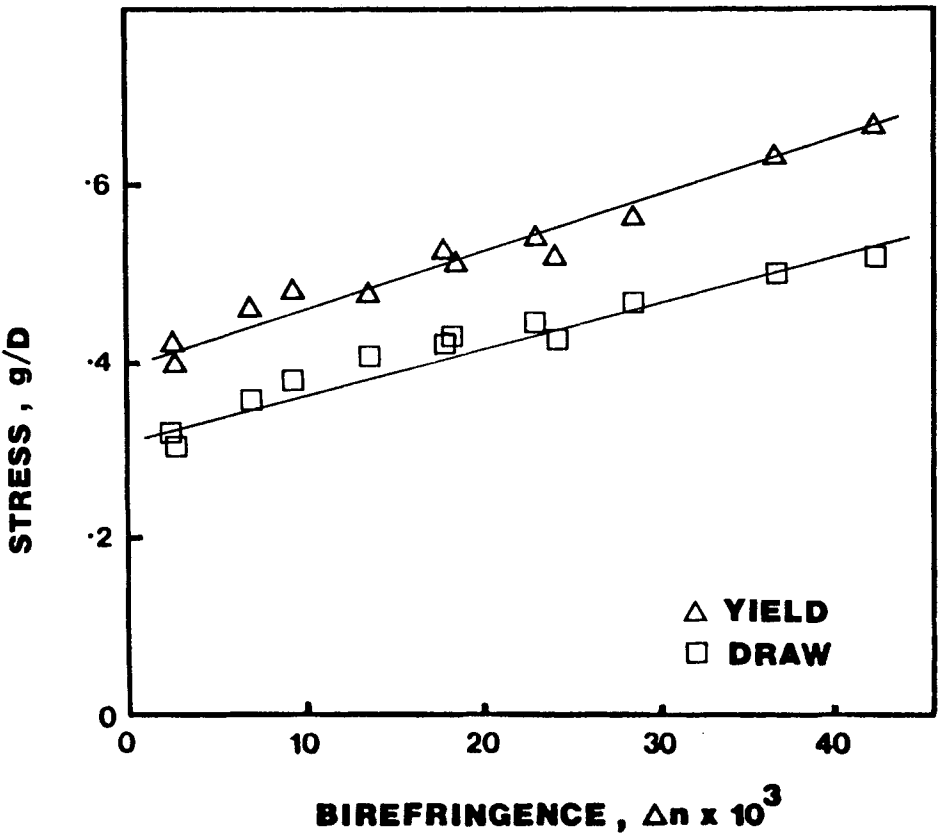

Fig. 13. Yield and draw loads versus birefringence for fibers spun at various wind-up speed and quench-air temperatures.

criminate between the two feasible proposals based only on the increase in the modulus and the overall orientation. However, analysis of DSC behavior (Fig. 6) and density measurements (Fig. 8) strongly suggest that structural evolution involves the growth of crystalline entities. Employing heat of fusion of 28.1 cal/g,[27] a percent crystallinity obtained from the excess enthalpy (i.e., the difference between the endotherm and the exotherm), is plotted as a function of WUS (Fig. 16). Clearly, the development of considerable crystallinity in this regime is a plausible proposition.

A similar relationship is deduced from density measurements (Fig. 8) and is shown in Figure 17. A two-phase model is invoked[28] in which the crystalline and amorphous densities were taken as 1.455 g/cc, and 1.335 g/cc.[29] The evidence presented here certainly supports the view that a distinct crystalline phase develops in the fiber within the entire range of WUS. The agreement between the crystallinity—WUS relationship (Figs. 16 and 17) appears to lend further support to our conclusion.

If the notion of semicrystalline structure is admissible, the natural draw ratio (Figs. 9 and 14) should reflect the relative magnitude of both components. The onset of redrawing (end of natural draw) signals the end of drawing of the "softer" component. Dependence of the draw ratio on WUS

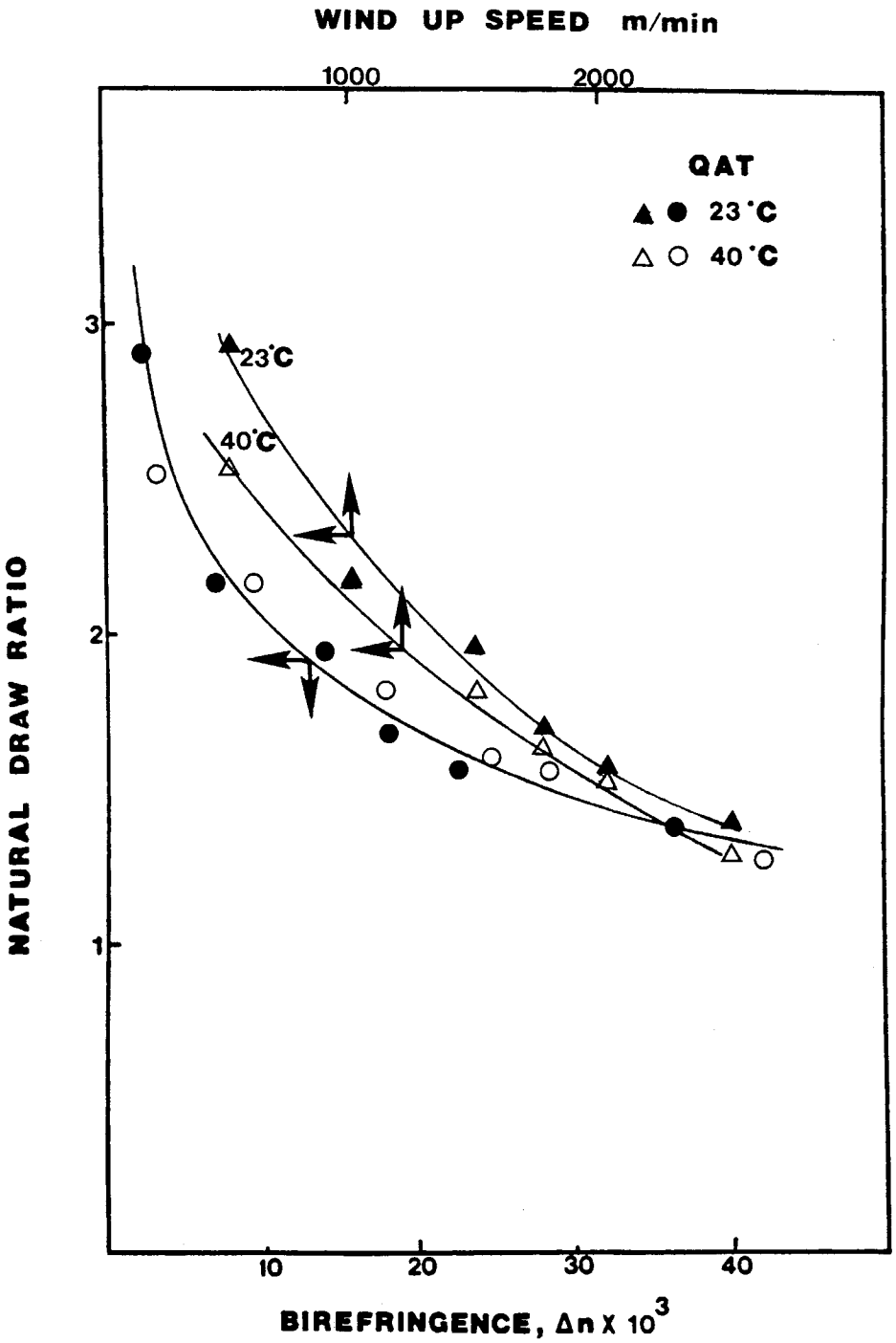

Fig. 14. The natural draw ratio (NDR) versus birefringence of fibers spun at various wind-up speed and quench-air temperature. The relationship between wind-up speed and natural draw ratio is also present.

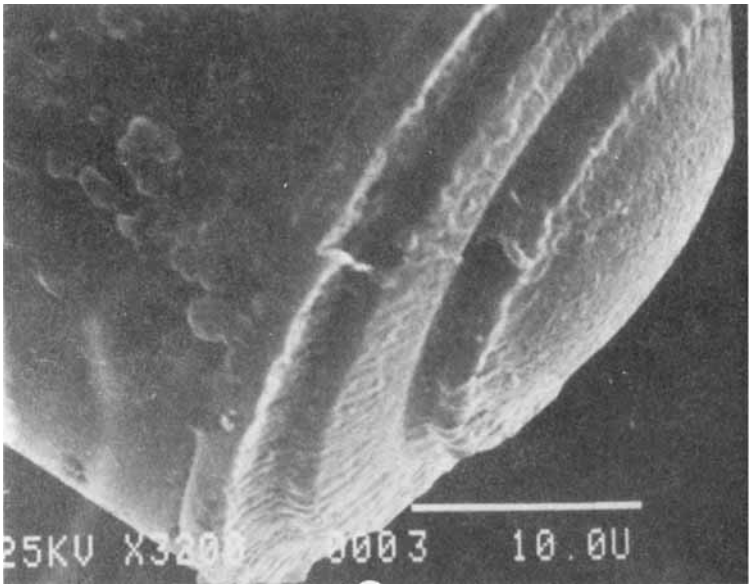

Fig. 15. SEM micrograph of a fiber spun at a wind-up speed of 500 m/min and a quench-air temperature of 23°C fractured under tension in liquid nitrogen.

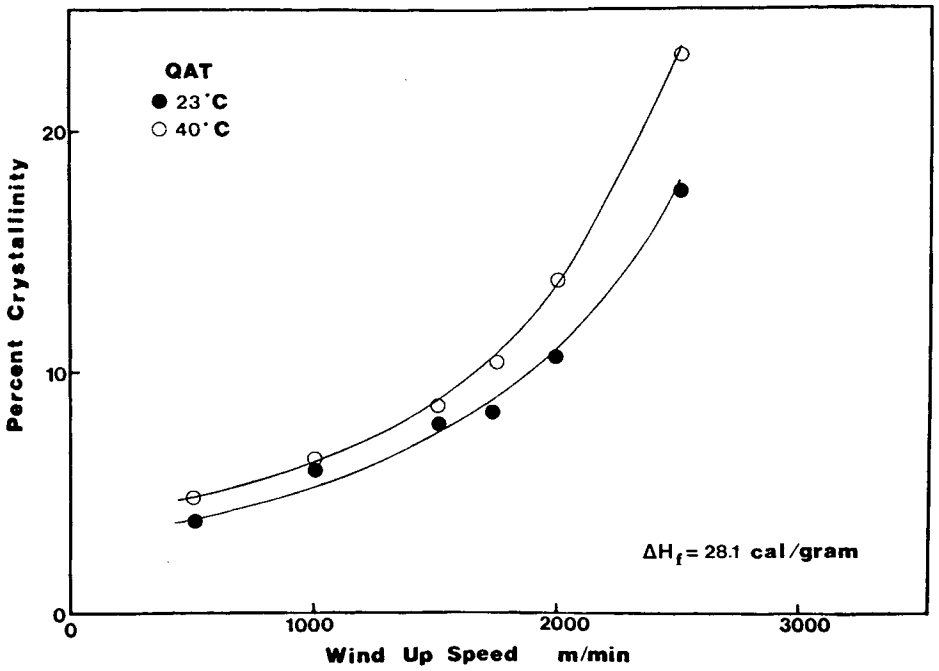

Fig. 16. The percent crystallinity of as-spun fibers as measured from calorimetry versus wind-up speed and the quench-air temperature.

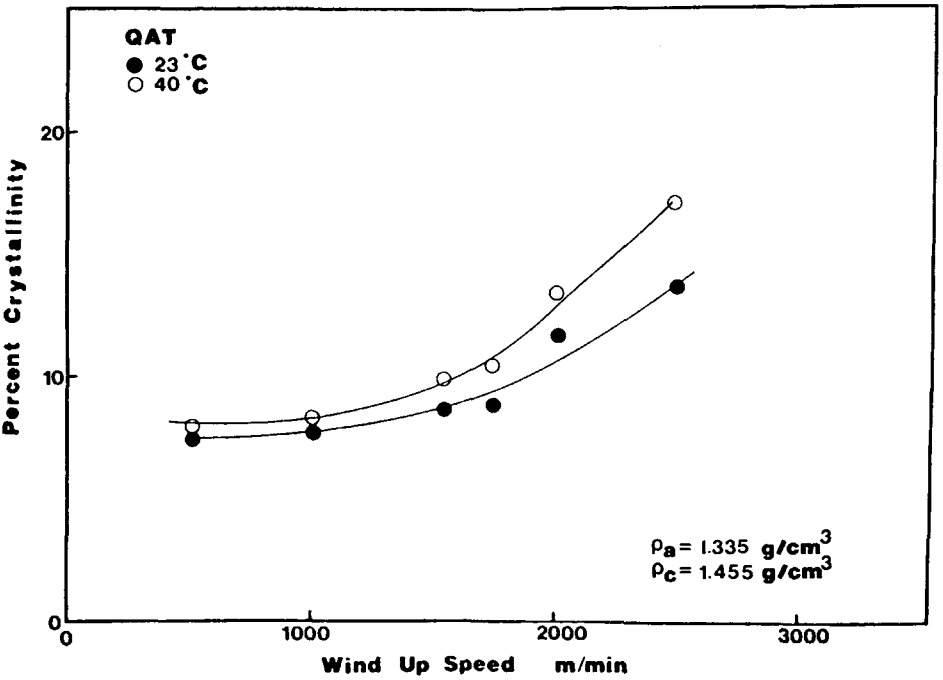

Fig. 17. The percent crystallinity of as-spun fibers as measured from the density versus the wind-up speed and quench-air temperature.

may imply that an increased amount of a hard phase, possibly crystallites, develops at higher spinning rates.

Evolution of the WAXD patterns (Fig. 5) does not yield an unambiguous picture about the crystallites. The crystallites are far from perfect. It is understood that constraints imposed on fiber melt spinning limit the size and morphology of the evolving crystallites and thus it becomes difficult to resolve their shapes and distribution. However, examining the mechanisms of drawing (irreversible deformation) could enable us to draw some idea about the relative size of the crystallites. A small crystallite (harder domain) may act as a stress concentrator. Such "inclusion" is incapable of supporting load, but concentrates normal stress which can cause normal deformation bands [Fig. 18(A)]. As these crystalline entities grow, they reach a size at which they become load-bearing. Hence, they can displace past one another yielding shear deformation bands [Fig. 18(B)]. Such load-bearing entities should obviously be three-dimensional. Indeed, normal deformation bands are the dominant drawing mechanism of fibers spun at lower speeds (Fig. 10) and shear deformation bands predominate fibers spun at higher WUS (Fig. 11). Therefore, it appears convincing to suggest that the increased crystallinity is, at least in part, due to increased crystallite size.

Considering all the evidence presented above, it is reasonable to propose that the structure of melt-spun PET fibers, even at low speeds, is made of imperfect crystalline domains embedded in amorphous matrix. Apparently, the crystallites grow larger and the amorphous matrix progressively be-

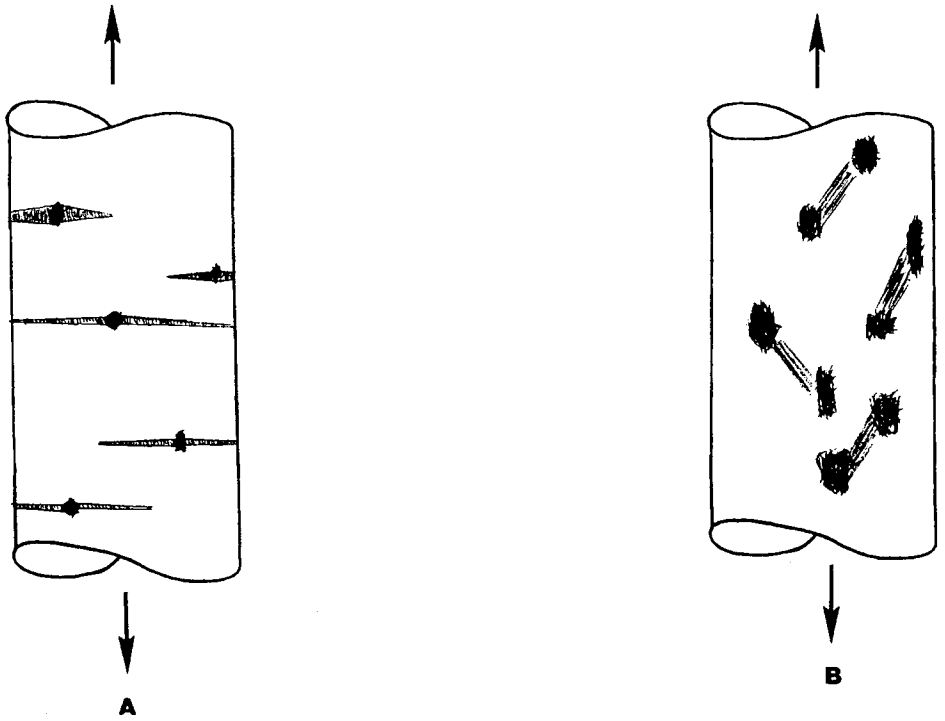

Fig. 18. Proposed deformation model based on structure analysis. Normal deformation zones are formed (a) when hard domains present act as stress concentrators. At high percent crystallinity, the hard domains act as load-bearing structures and a shear type of deformation is observed (b).

comes more oriented as the spinning speed increases. Interestingly enough, while this paper was in preparation, Harburn and co-workers[30] proposed a closely similar model for drawn PET fibers as a result of rigorous analysis of optical transforms from WAXS and SAXS patterns.

We must bear in mind that the model proposed here envisages the fiber as a continuum. Scanning electron micrographs of fibers fractured in liquid Nitrogen (Fig. 15) clearly show the structural variance induced radially during spinning. This added complexity could be influential in determining the ultimate fiber properties.

The authors wish to thank the Goodyear Tire and Rubber Company for providing the melt-spun fibers and for the financial assistance provided through the Center for Applied Polymer Research at Case Western Reserve University. We would also like to thank Dr. A. Chudnovsky of Case Western Reserve University and Drs. B. W. Pengilly and W. Perkins of Goodyear for their suggestions and comments during this work.

References

1. G. E. Hagler, *Polym. Sci. Eng.*, **21(3)**, 121 (1981).
2. A. Ziabicki, *Sen'i Gakkaishi*, **38**, 409 (1982).
3. S. K. Garg, *J. Appl. Polym. Sci.*, **29**, 2111 (1984).
4. H. M. Heuvel and R. Huisman, *J. Appl. Polym. Sci.*, **22**, 2229 (1978).
5. J. Shimizu, K. Toriumi, and K. Tamai, *Sen'i Gakkaishi*, **33**, T208 (1977).

6. P. Desai and A. S. Abhiraman, *J. Polym. Sci., Polym. Phys. Ed.*, **23**, 653 (1985).
7. M. Sotton, A. Arniaud, and C. Rabourdin, *J. Appl. Polym. Sci.*, **22**, 2585 (1978).
8. G. W. Davis, A. E. Everage, and J. R. Taibot, *Fiber Producers*, Feb., (1984) page 22.
9. W. Perkins, private communications (1984).
10. E. A. Turi, Ed., *Thermal Characterization of Polymeric Materials*, Academic Press, New York, 1981, pp. 771–772.
11. H. H. George, A. Holt, and A. Buckley, *Polym. Eng. Sci.*, **23**, 95 (1983).
12. A. Hamidi, A. S. Abhiraman, and P. Asher, *J. Appl. Polym. Sci.*, **28**, 567 (1983).
13. G. Bragato and G. Gianotti, *Eur. Polym. J.*, **19**, 795 (1983).
14. A. Ziabicki and K. Kedzierska, *J. Appl. Polym. Sci.*, **6(19)**, 111 (1962).
15. V. E. Liska, *Kolliod-Z*, **251**, 1028 (1973).
16. S. Fakirov, E. W. Fischer, R. Hoffman, and G. F. Schmidt, *Polymer*, **18**, 1121 (1977).
17. P., J. Holdsworth and A. Turner-Jones, *Polymer*, **12**, 195 (1971).
18. H. Brody, *J. Macromol. Sci., Phys.*, **B 22 (3)**, 407 (1983).
19. D. Ihm and J. Cuculo, *J. Macromol. Sci., Rev. Macromol. Chem. Phys.*, **C 24 (3)**, 419 (1984).
20. J. Shimizu, N. Okui, T. Kikutani, A. Ono, and A. Takaku, *Sen'i Gakkaishi*, **37**, T135, (1981).
21. G. P. Andranova, B. A. Arutyunov, and Yu V. Popov, *J. Polym. Sci., Phys. Ed.*, **16**, 1139 (1978).
22. T. Pakula and E. W. Fischer, *J. Polym. Sci., Polym. Phys. Ed.*, **19**, 1705 (1981).
23. I. M. Ward, *J. Macromol. Sci., Phys.*, **B1 (4)**, 667 (1967).
24. S. Lee, H. Mayaji, and P. H. Geil, *J. Macromol. Sci., Phys.*, **B22 (3)**, 489 (1983).
25. P. H. Geil, *Polymer Single Crystals*, R. E. Krieger Pub., Huntington, New York, 1973.
26. P. Lindenmeyer, *Text. Res. J.*, **50**, 395 (1980).
27. C. W. Smith and M. Dole, *J. Polym. Sci.*, **20**, 37 (1956).
28. R. J. Samuels, *Structured Polymer Properties*, John Wiley and Sons, New York, 1974.
29. S. K. Garg, *J. Appl. Polym. Sci.*, **27**, 2857 (1982).
30. G. Harburn, J. W. Lewis, and J. O. Warwicker, *Polymer*, **26**, 469 (1985).

Received September 16, 1985
Accepted January 13, 1986